JOURNAL OF PROPULSION AND POWER
Vol. 11, No. 2, March–April 1995

Study of the Flow Turning Loss in a Simulated Solid Rocket Motor

Lawrence M. Matta* and Ben T. Zinn†
Georgia Institute of Technology, Atlanta, Georgia 30332

The flow turning loss, one of the processes that damp instabilities in solid rockets, is caused by the interaction of the axial acoustic field in an unstable motor with the flow of combustion products from the propellant surface. While state-of-the-art stability models generally account for the flow turning loss, its characteristics have never been fully investigated. In order to study the contribution of the flow turning loss to acoustic stability, a one-dimensional acoustic stability equation that includes the flow turning loss term was derived, providing the theoretical background and expressions needed to guide an experimental study. Experiments were performed to determine the dependence of the flow turning loss upon the injection and mean-flow Mach numbers and the location of the flow turning region relative to the standing acoustic wave. These studies showed that the flow turning loss strongly depends upon the magnitude of the gas velocity at the propellant surface and the location of the flow turning region relative to the standing pressure wave. A simple numerical simulation of the experimental setup was developed and its predictions were found to agree well with the measured data.

Nomenclature

a	=	speed of sound
E^2	=	quantity representative of the total acoustic energy in the cavity
H	=	height of two-dimensional duct used in analysis
h_T	=	total specific enthalpy
$\hat{\imath}$	=	unit vector in the axial x direction
$\hat{\jmath}$	=	unit vector in the transverse y direction
L	=	length of duct
$\dot{m}$	=	mass flux rate
u	=	axial, x direction, component of velocity
$\mathbf{V}$	=	velocity vector
v	=	transverse, y direction, component of velocity

Subscripts

b	=	value at side wall
t	=	average over time
y	=	average over the y direction
0, 1, 2	=	acoustic order

Introduction

THE goal of this research effort was to develop a better understanding of the flow turning loss and related flow processes that contribute to the driving and damping of axial instabilities in solid propellant rocket motors. An understanding of these processes is necessary for the development of dependable techniques for designing stable solid propellant rocket motors.

The occurrence of combustion instabilities is controlled by the relative magnitudes of the driving and damping mechanisms within the combustor that add and remove energy from the oscillations, respectively. If the acoustic energy gains outweigh the losses, disturbances amplify to levels that can adversely affect guidance, thrust history, and structural integrity of the motor.[1–4] Because of the high energy densities and comparatively low losses observed in most combustors designed for use in propulsion systems, the possibility of encountering instability is high. Combustion instability is a common problem in solid propellant rocket motors, and because it can lead to system and/or mission failure, the development of reliable methods for predicting the stability of solid propellant rocket motors has been a long-standing goal of the propulsion community.

In order to eliminate or reduce the severity of acoustic oscillations resulting from combustion instabilities in solid rocket motors, the mechanisms by which energy is added to and removed from these oscillations must be identified and understood. The energy necessary to initiate and maintain the instability is generally provided by the interaction of the solid propellant combustion process with the acoustic oscillations present in the motor. On the other hand, processes such as acoustic energy transmission through the choked nozzle and out of the motor, viscous dissipation, and flow turning, generally remove energy from the oscillations, thus stabilizing the motor. While viscous damping is generally neglected in rocket stability analyses, and much information exists about nozzle damping and driving by the combustion process, relatively little is known about the flow turning loss.

Combustion products generally leave a burning solid propellant normal to the surface with no axial velocity. These gases acquire axial velocity as they move away from the propellant surface and are entrained in the motor's core flow. During this turning process, the combustion products acquire axial acoustic energy from the core flow oscillations. This phenomena was first discussed by Culick[5–8] who argued that since the combustion products entering the core flow acquire axial acoustic energy from the existing, axial, core flow oscillations, the axial acoustic field experiences a loss of acoustic energy that tends to damp the oscillations and, thus, stabilize the system. The existence of the flow turning loss and its physical interpretation have been somewhat controversial.

Studies of the flow turning phenomenon have been undertaken by a number of researchers, including experimental studies by Hersch[9,10] and Chen[11] and analytical investigations by Baum[12,13] and Hegde.[14–16] In the cited studies, the behavior of acoustic fields in a channel in which the solid propellant combustion process was simulated by mass addition through side walls was investigated. Hersch used pressure measurements upstream and downstream of a region of wall injection to determine the influence of flow turning. Hersch's

Presented as Paper 93-0115 at the AIAA 31st Aerospace Sciences Meeting, Reno, NV, Jan. 11–14, 1993; received Dec. 11, 1993; revision received June 30, 1994; accepted for publication Aug. 17, 1994.

*Postdoctoral Research Fellow, Department of Aerospace Engineering. Member AIAA.
†David S. Lewis Chair and Regents Professor, Department of Aerospace Engineering. Fellow AIAA.

measurements showed that the flow turning loss depended upon the frequency of oscillation and that it was not linearly dependent upon the injection velocity; conclusions that were inconsistent with the behavior of the flow turning loss as predicted by Culick.[5-8] Chen[11] measured the acoustic intensity flux through the boundaries of a control volume in the flow turning region to determine the damping due to flow turning. In cold flow studies, Chen determined that the magnitude of the flow turning loss did not depend upon where the mass was injected with respect to the standing acoustic wave. The accuracy of the results of both Hersch's and Chen's investigations are open to question, because neither of these indirect measurement techniques could distinguish the effects of the flow turning loss term from a number of other mean velocity-dependent effects that always appears in the cavity stability equation together with the flow turning loss.

Baum's computational studies[12,13] show that the flowfield near the wall is extremely complex, involving interactions between a multitude of vortical structures and energy exchange between the mean flow and the oscillations. Hegde et al.[14-16] used a linear analysis and hot wire measurements to determine the acoustic characteristics and losses of a duct containing a standing axial acoustic wave and mass addition through a side wall. This investigation tested the validity of a linear model similar to those currently used to predict solid propellant rocket stability and performance, and in contrast with Baum's results it suggests that a linear model may adequately describe the important features of the flow turning loss.

The objective of this research was to investigate the behavior of the flow turning loss term that is included in currently used one-dimensional linear stability prediction codes and to measure it. First, a one-dimensional acoustic stability equation that includes the flow turning loss term was derived by an approach different from Culick's to guide the experimental study. Experiments were then performed to measure the effect of operating conditions (e.g., the injection and core flow velocities and the location of injection relative to the standing pressure wave) upon the flow turning loss term in the stability equation. Finally, a simple numerical simulation of the experimental setup was performed and the results were compared to the experimental data.

Theoretical Study

To provide a foundation for the experimental study and to verify the existence of the flow turning loss term, an equation that describes the acoustic stability of a combustor was derived by an approach independent from the one used by Culick.[5] The developed formulation is based upon the acoustic energy conservation approach developed by Cantrell and Hart,[17] who used the second-order conservation equations to predict the stability of acoustic oscillations in arbitrary volumes with mean flow, and a similar approach used by Flandro[18] was also a basis of the formulation. Because the study is focused upon the term of the one-dimensional stability equation known as the "flow turning loss," the equations used in the analysis are averaged over the cross-sectional area of the chamber. While the averaging process seems counterproductive by obscuring the physics of a problem that is multidimensional in nature, it is necessary because the flow turning loss term does not appear decoupled from related terms unless the problem is one dimensionalized.

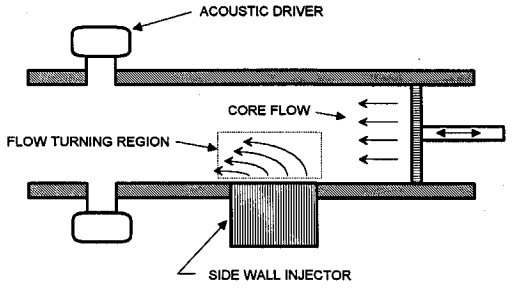

Fig. 1 Schematic of the experimental setup utilized in the investigation of the flow turning loss.

The analysis begins with considerations of the mass, momentum, and energy conservation equations. In order to make the investigation as straightforward as possible, and make it applicable to the experimental setup shown in Fig. 1, the investigated geometry consisted of a two-dimensional rectangular duct of height H and length L. The two-dimensional mass and momentum conservation equations are as follows:

Mass

$$\frac{\partial \rho}{\partial t} + \nabla \cdot \dot{m} = 0 \tag{1}$$

Momentum

$$\frac{\partial \boldsymbol{V}}{\partial t} + \nabla\left(\frac{\boldsymbol{V}\cdot\boldsymbol{V}}{2}\right) + \frac{1}{\rho}\nabla p = \left(u\frac{\partial u}{\partial y}\right)\hat{\jmath} + \left(v\frac{\partial v}{\partial x}\right)\hat{\imath} - \left(\frac{\partial v}{\partial x}\right)\hat{\jmath} - \left(v\frac{\partial u}{\partial y}\right)\hat{\imath} \tag{2}$$

where ρ is the density, u and v are the axial and vertical components of the velocity vector, p is the pressure, and $\dot{m}$ is the mass flux vector $\rho \boldsymbol{V}$. This particular form of the momentum equation has been chosen for its convenience later in the analysis. Assuming that the flow is isentropic, Eq. (2) can be rewritten as

$$\frac{\partial \boldsymbol{V}}{\partial t} + \nabla h_T = \left(u\frac{\partial u}{\partial y}\right)\hat{\jmath} + \left(v\frac{\partial v}{\partial x}\right)\hat{\imath} - \left(u\frac{\partial v}{\partial x}\right)\hat{\jmath} - \left(v\frac{\partial u}{\partial y}\right)\hat{\imath} \tag{3}$$

where h_T is the total enthalpy per unit mass. As a result of the isentropic flow assumption, this analysis does not account for such processes as particle damping and heat transfer, and gas-phase heat addition by combustion.

The development of the acoustic stability equation by an energy balance approach starts with the following form of the energy equation:

$$\frac{\partial}{\partial t}(\rho h_T - p) = -\nabla \cdot (\dot{m} h_T) \tag{4}$$

Since the acoustic energy is a second-order acoustic quantity, all first- and second-order terms must be retained in the analysis, whereas third- and higher-order terms may be neglected in a linear analysis. Thus, expanding Eq. (4) to second-order and time-averaging the resulting equation yields:

$$\left\langle \frac{\partial}{\partial t}(\rho h_T - p)_2 \right\rangle_t = -\langle \nabla \cdot (\dot{m}_2 h_{T0}) + \nabla \cdot (\dot{m}_1 h_{T1}) + \nabla \cdot (\dot{m}_0 h_{T2}) \rangle_t \tag{5}$$

where the quantities inside braces $\langle\ \rangle$ are averaged over the subscripted variable, and the numerical subscripts indicate the term's order.

To eliminate the dependence upon the transverse dimension y, Eq. (5) is averaged over the height (i.e., in the y direction) of the constant area duct to obtain

$$\left\langle \frac{\partial}{\partial t}(\rho h_T - p)_2 \right\rangle_{t,y} = -\frac{\partial}{\partial x}\langle (\rho u)_2 h_{T0} + (\rho u)_1 h_{T1} + (\rho u)_0 h_{T2} \rangle_{t,y} - \frac{1}{H}\langle [(\rho v)_2 h_{T0} + (\rho v)_1 h_{T1} + (\rho v)_0 h_{T2}]_0^H \rangle_t \tag{6}$$

Equation (6) includes second-order terms that are generally not known and are difficult to determine. It is possible, however, to use the continuity and momentum equations, Eqs. (1) and (3), to eliminate these terms in Eq. (6). In order to accomplish this, some manipulation of Eqs. (1) and (3) must be performed. With this in mind, the zeroth-order part of Eq. (3) (i.e., the steady-state energy equation) is obtained by retaining all terms that are independent of time and neglecting terms of second-order and higher in the mean Mach number, resulting in the following equation:

$$\nabla h_{T0} = 0 \tag{7}$$

Next, the continuity equation [Eq. (1)] was multiplied by ∇h_{T0} and the resulting equation added to the product of Eq. (7) and $\dot{m}$. The resulting equation was then averaged over y and t to obtain the following equation where all terms of the order of Mach number square or higher were neglected:

$$\frac{\partial}{\partial x}\langle(\rho u)_2 h_{T0}\rangle_{t,y} + \frac{1}{H}\langle[(\rho v)_2 h_{T0}]_0^H\rangle_t = -\left\langle h_{T0}\frac{\partial \rho_2}{\partial t}\right\rangle_{t,y} \tag{8}$$

Another needed equation is obtained by forming the dot product of the second-order momentum equation [Eq. (3)] with the zeroeth-order mass flux to obtain the following expression where all terms of the order of the Mach number squared or higher were neglected:

$$\langle\nabla\cdot(\dot{m}_0 h_{T2})\rangle_t + \left\langle\frac{\partial}{\partial t}(\dot{m}_0\cdot V_2)\right\rangle_t = \left\langle\left(\rho_0 v_0 u_1\frac{\partial u_1}{\partial y}\right) + \left(\rho_0 u_0 v_1\frac{\partial v_1}{\partial x}\right) - \left(\rho_0 v_0 u_1\frac{\partial v_1}{\partial x}\right) - \left(\rho_0 u_0 v_1\frac{\partial u_1}{\partial y}\right)\right\rangle_t \tag{9}$$

Equation (9) is now averaged across the duct to yield

$$\frac{\partial}{\partial x}\langle(\rho u)_0 h_{T2}\rangle_{t,y} + \frac{1}{H}\langle[(\rho v)_0 h_{T2}]_0^H\rangle_t + \left\langle\frac{\partial}{\partial t}(\rho_0 u_0 u_2 + \rho_0 v_0 v_2)\right\rangle_{t,y} = \left\langle\left(\rho_0 v_0 u_1\frac{\partial u_1}{\partial y}\right) + \left(\rho_0 u_0 v_1\frac{\partial v_1}{\partial x}\right) - \left(\rho_0 v_0 u_1\frac{\partial v_1}{\partial x}\right) - \left(\rho_0 u_0 v_1\frac{\partial u_1}{\partial y}\right)\right\rangle_{t,y} \tag{10}$$

Equations (8) and (10), while physically not meaningful, are in forms that are useful for simplifying the energy equation [Eq. (6)]. By substituting Eqs. (8) and (10) into Eq. (6), rearranging and simplifying the resulting expression, and integrating the result over the length of the duct, the following equation is obtained:

$$\frac{\partial}{\partial t}\int_0^L\left\langle\frac{p_1^2}{2\rho_0 a_0^2} + \frac{p_1 u_0 u_1}{a_0^2} + \frac{\rho_0 u_1^2}{2}\right\rangle_{t,y} dx = -\left\langle\left[p_1 u_1 + \frac{p_1^2 u_0}{\rho_0 a_0^2} + \rho_0 u_0 u_1^2\right]_0^L\right\rangle_{t,y} - \left\langle\frac{1}{H}\int_0^L\left(\langle p_1\rangle_y[v_1]_0^H + \left\langle\frac{p_1}{\rho_0 a_0^2}\right\rangle_y[v_0 p_1]_0^H\right)dx\right\rangle_t - \left\langle\frac{1}{H}\int_0^L(\langle\rho_0 u_1\rangle_y[v_1 u_0]_0^H + \langle\rho_0 u_1\rangle_y[v_0 u_1]_0^H)\,dx\right\rangle_t + \left\langle\frac{1}{H}\int_0^L\langle\rho_0 u_1^2\rangle_y[v_0]_0^H\,dx\right\rangle_t \tag{11}$$

where a_0 is the zeroth-order speed of sound. Equation (11) is the integral form of an equation for the quantity in the time derivative. It should be pointed out that this quantity, which has units of energy, does not represent the total acoustic energy of the system. The lack of a simple physical interpretation of this quantity is the unfortunate result of the cancellations that resulted from the above described derivation of Eq. (11).

Letting, for convenience, the energy integral on the left side of Eq. (11) equal E^2; i.e.,

$$E^2 = \int_0^L\left\langle\frac{p_1^2}{2\rho_0 a_0^2} + \frac{p_1 u_0 u_1}{a_0^2} + \frac{\rho_0 u_1^2}{2}\right\rangle_{t,y} dx \tag{12}$$

and noting that the growth rate of each of the acoustic energy terms is the same as the growth rate of E^2, then the exponential growth rate α can be obtained using the following expression:

$$2\alpha = = \left\langle\frac{\partial\Psi}{\partial t}\right\rangle_t \Big/ \langle\Psi - \Psi_0\rangle_t \tag{13}$$

where Ψ is a second-order acoustic quantity. Using Eqs. (12) and (13), the following acoustic stability equation is obtained from Eq. (11):

$$2\alpha E^2 = -\left\langle\left[p_1 u_1 + \frac{p_1^2 u_0}{\rho_0 a_0^2} + \rho_0 u_0 u_1^2\right]_0^L\right\rangle_{t,y} - \left\langle\frac{1}{H}\int_0^L\langle p_1\rangle_y\left[\frac{\dot{m}_{b1}}{\rho_0}\right]_0^H dx\right\rangle_t - \left\langle\frac{1}{H}\int_0^L\left(\langle u_1\rangle_y[\dot{m}_{b1}u_0]_0^H + \langle u_1\rangle_y[\dot{m}_{b0}u_1]_0^H - \langle u_1^2\rangle_y[\dot{m}_{b0}]_0^H\right)dx\right\rangle_t \tag{14}$$

where $\dot{m}_b$ is the mass flux (ρv) out of the walls (where all burning is assumed to take place), which is by definition positive in the positive y direction. This equation is by intent (and not by any obvious choice of groupings) of a form that allows comparison with the acoustic stability equation developed by Culick.[5] Culick's equation, simplified by removing the terms that contain the effects of particulate matter, gas phase combustion, and cross-duct temperature gradients, is

$$2\alpha E_c^2 = -\left\langle\left[\hat{p}_l\hat{u}_l + \frac{\hat{p}_l^2 u_0}{\rho_0 a_0^2}\right]_0^L\right\rangle_y - \frac{1}{H}\int_0^L\langle\hat{p}_l\rangle_y\left[\frac{\hat{m}_b}{\rho_0}\right]_0^H dx - \frac{1}{H}\int_0^L\left(\langle\hat{u}_l\rangle_y[\hat{m}_b u_0]_0^H + \langle\hat{u}_l\rangle_y[\dot{m}_{b0}u_l]_0^H - \langle\hat{u}_l^2\rangle_y[\dot{m}_{b0}]_0^H\right)dx \tag{15}$$

where $\hat{}$ represents the amplitude of an oscillatory quantity, and the subscript l signifies approximate solutions for the acoustic pressure and velocity, which are solutions of the classical acoustic problem governed by the following equations and boundary conditions:

$$\frac{\partial^2\hat{p}_l}{\partial x^2} + k_l^2\hat{p}_l = 0 \tag{16}$$

$$\rho_0\frac{\partial u_l}{\partial t} + \frac{\partial p_l}{\partial x} = 0 \tag{17}$$

$$\frac{d\hat{p}_l}{dx} = 0, \qquad (x = 0, L) \tag{18}$$

Comparison of Eqs. (14) and (15) reveals that the term

$$\langle [\rho_0 u_0 u_1^2]_0^L \rangle_{t,y}$$

appears only in Eq. (14). Flandro[19] has demonstrated that this term is correctly placed in Eq. (14), and does not lead to results that are inconsistent with solutions of the linear problem carried out by other means. The term of Eq. (15) associated with the flow turning loss is also present in Eq. (14); i.e.,

$$\text{flow turning loss} = \left\langle \frac{1}{H} \int_0^L \langle u_1^2 \rangle_y [\dot{m}_{b0}]_0^H \, dx \right\rangle \qquad (19)$$

Consistent with the convention used for the transverse velocity component v, the mass flux at the side wall $\dot{m}_b$ is taken to be positive in the positive y direction (up), and negative in the negative y direction (down). Inspection of the expression in Eq. (19) shows that it is negative if mass enters the control volume through the top or bottom boundary, implying that it tends to reduce α and, thus, stabilize the system. On the other hand, if mass exits the control volume through the top or bottom boundary, the resulting expression is always positive, which increases α and destabilizes the system.

It should be noted that if the flow is irrotational, as was assumed by Cantrell and Hart,[17] the right side of Eq. (3) is identically zero. When this is the case, the flow turning term does not appear in the stability equation.

Experimental Study

In this phase of the study, the dependence of the flow-turning loss term of the developed acoustic stability equation upon the core flow and wall injection velocities and position of flow turning region with respect to the standing axial acoustic wave was investigated experimentally. The flow turning loss term was determined by measuring the distributions of the mean velocities, acoustic velocities and pressures within the flow turning region, and substituting the measured data into the derived acoustic stability equation [Eq. (14)]. A schematic of the utilized experimental setup is presented in Fig. 1. The setup allows the study of the effect of a tangentially injected flow upon a standing acoustic field representing an axial instability in a motor. The developed setup consisted of a 7.6-cm-high × 3.8-cm-wide × 3-m-long rectangular steel duct with an injector mounted on the bottom wall. The wall mounted injector consisted of 1537 stainless steel tubes, 0.762 mm i.d., arranged in a 53 × 29 rectangular matrix with a 0.1-mm spacing. Two acoustic drivers mounted on opposing duct walls just upstream of the exit plane were used to excite a standing acoustic wave in the duct that simulates an axial instability in a rocket motor. A porous injector (sintered stainless steel) was used to inject a mean flow that simulated the core flow in a solid rocket motor. The core flow injector was moveable, so that the location of the wall-mounted injector (and, therefore, the flow turning region) relative to the standing acoustic wave can be varied by axial translation of the core flow injector. Velocity measurements were performed using an LDV system through quartz windows in the side walls adjacent to the wall-mounted injector. Details of the data acquisition technique used with the LDV are discussed in Refs. 11 and 19. Acoustic pressures were measured with a microphone attached to a probe that was inserted through the exhaust port.

The flow turning loss was determined by measuring the acoustic pressure and velocity distributions in the region above the wall injector and substituting the resulting data into Eq. (14). A typical mean velocity field measured in a point in such a region is shown in Fig. 2, where the core flow was injected from the right, the wall-mounted injector was on the bottom, and the acoustic drivers were located downstream (to the left) of the investigated control volume. Typical measured acoustic velocity vectors, measured at various phases of an oscillation cycle, are shown in Fig. 3. The acoustic intensity vector field for this configuration, described in Fig. 4, shows that for these test conditions a relatively large fraction of the acoustic intensity is directed into (i.e., absorbed by) the wall mounted injector, which is not choked. This occurs because the pressure oscillations above the injector drive the oscillatory mass flow through the injector. When the injector is located near an acoustic pressure antinode, the amplitude of the pressure oscillation above the injector, and therefore, the amplitude of the unsteady mass flow, is maximized. Conversely, when the injector is located at an acoustic pressure node, the mass flow through the injector is nearly steady. The acoustic response of the injector limits the similarity between the experiment and an actual solid propellant motor. The flow of "classical acoustic intensity" into the burner represents a zeroeth-order (in Mach number) acoustic energy loss in the one-dimensional acoustic stability equation [Eq. (14)]. While this effect is significant to the acoustic growth rate, it is not directly related to the flow turning loss term.

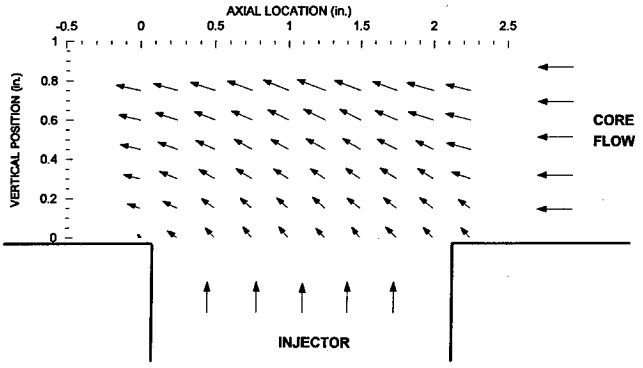

Fig. 2 Vector plot of typical measured mean velocity field in the flow turning region.

The dependence of the flow turning loss upon various design parameters was investigated by determining the dependence of α_{FTL}, defined as

$$\alpha_{\text{FTL}} = \left\langle \frac{1}{H} \int_0^L \langle u_1^2 \rangle_y [\dot{m}_{b0}]_0^H \, dx \right\rangle_t \Big/ 2\alpha E^2 \qquad (20)$$

which describes the linear contribution of the flow turning loss to the overall acoustic stability of the cavity, upon these parameters. Due to the large amount of time required to acquire the necessary velocity and pressure data for each configuration and the sensitivity of the flowfield to experimental conditions, only a small number of data per configuration (generally three) were collected. To compensate, a large number of experimental runs were performed, and trends were determined by comparing a number of results. Errors in the measurements are on the order of 5% of the measured value. While this error may be significant enough to affect the interpretation of the trend of data from a single experiment, determining trends from the results from a number of tests minimizes the effect of measurement errors.

The results of one experimental run, displayed in Fig. 5, shows the effect of the side wall injection velocity upon α_{FTL} in the investigated region. The results were obtained in a test conducted with a frequency of 550 Hz, a mean core flow velocity of 0.4 m/s, and injection at a pressure node. The measured α_{FTL} varies linearly with the mean side wall injection velocity.

Figure 6 shows the dependence of α_{FTL} in the investigated region upon the mean core flow velocity. This test was conducted with a frequency of 550 Hz, a side wall injection velocity of 0.156 m/s, and the burner located at a pressure node. The measured α_{FTL} increase with the mean core flow velocity.

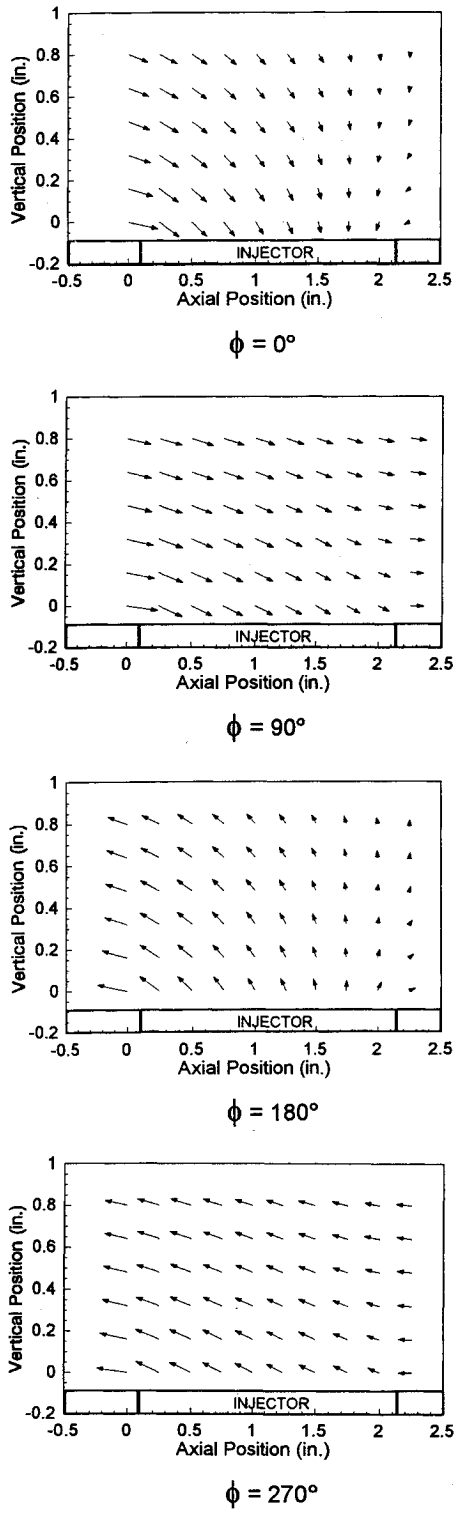

Fig. 3 Typical measured acoustic velocity vector field at various phases of one cycle of oscillation.

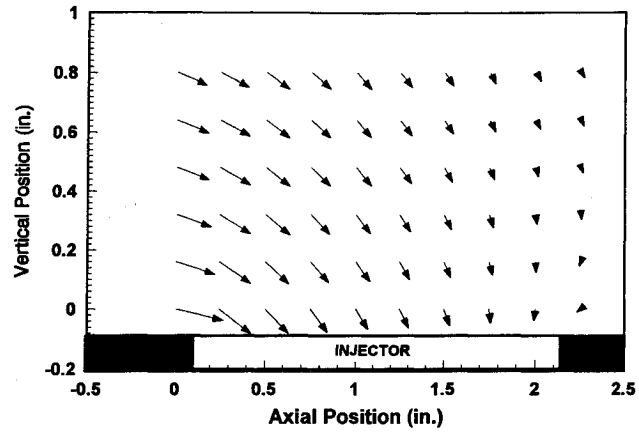

Fig. 4 Diagram of typical measured acoustic intensity vectors $\langle p'V' \rangle_t$.

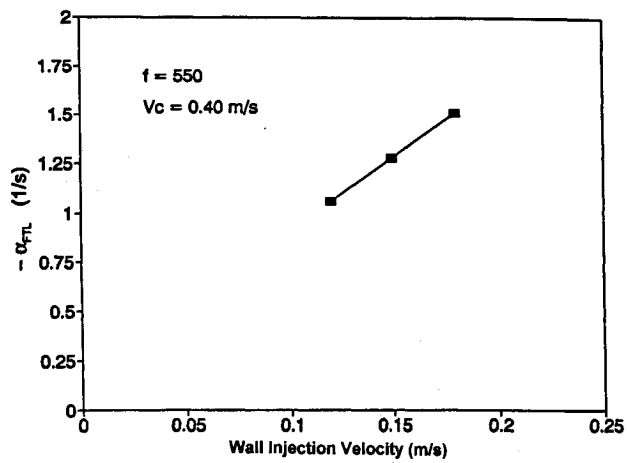

Fig. 5 Results of an experiment showing the effect of side wall injection velocity upon α_{FTL}.

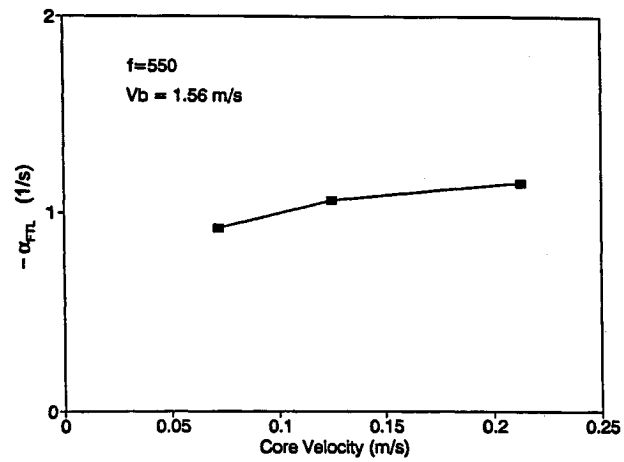

Fig. 6 Results of an experiment showing the effect of mean core flow velocity upon α_{FTL}.

The trend of these data and the results of other tests (because a conclusion cannot be drawn from three data points) shows that α_{FTL} appears to approach a limit value as the core velocity increases. This is due to incomplete turning of the flow inside the investigated region. In the experimental study, the investigated control volume does not extend from the burner surface to the top wall. Inspection of the mean velocity profile shown in Fig. 2 reveals that the flow at the top of the investigated control volume is not fully turned into the axial direction. As the core flow Mach number increases, flow turning is completed to a higher degree within the investigated control volume. Therefore, it is expected that as the core flow Mach number increases, the flow turning loss will also increase, which is consistent with the trend of the measured data.

The dependence of α_{FTL} upon the location of the flow turning region with respect to the standing acoustic wave is shown in Fig. 7. These data were obtained in experiments with a mean core velocity of 2.86 m/s, a mean wall injection velocity of 1.34 m/s, and a frequency of 550 Hz. The measured α_{FTL} was maximum when the flow turning occurred at an acoustic pressure node, and minimum when the flow turning region was located at a pressure antinode.

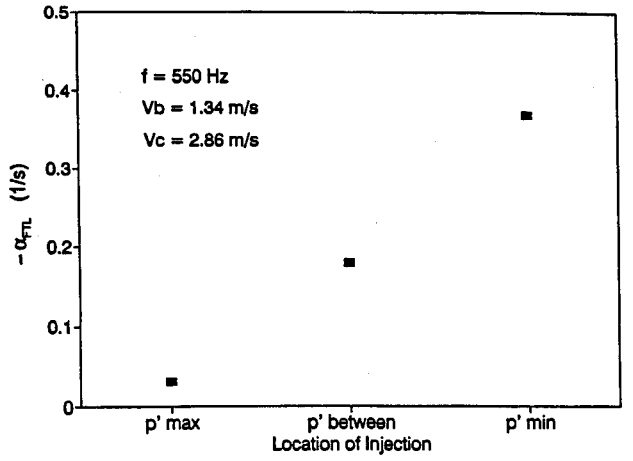

Fig. 7 Results of an experiment showing the effect of the location of the flow turning region relative to the standing acoustic wave upon α_{FTL}.

Numerical Simulation

The experimental setup used in the flow turning investigation was modeled numerically and the calculated results were compared with measured data. The simulation was performed using the following two-dimensional acoustic continuity and axial momentum equations for the experimental setup:

Mass

$$\frac{\partial \rho'}{\partial t} + \frac{\partial}{\partial x}(\bar{\rho}u' + \rho'\bar{u}) + \frac{\partial}{\partial y}(\bar{\rho}v' + \rho'\bar{v}) = 0 \quad (21)$$

Axial momentum

$$\bar{\rho}\frac{\partial u'}{\partial t} + \bar{\rho}\frac{\partial}{\partial x}(\bar{u}u') + \bar{\rho}\bar{v}\frac{\partial u'}{\partial y} + \bar{\rho}v'\frac{\partial \bar{u}}{\partial y} + \frac{\partial p'}{\partial x} = 0 \quad (22)$$

Where an overbar represents a time-averaged quantity, and a prime represents an acoustic quantity.

Averaging these equations over the width (y direction) of the constant area duct yields

$$\left\langle \frac{\partial \rho'}{\partial t} \right\rangle_y + \left\langle \frac{\partial}{\partial x}(\bar{\rho}u' + \rho\partial\bar{u}) \right\rangle_y = -\frac{1}{H}[\bar{\rho}' + \rho'\bar{v}]_0^H \quad (23)$$

$$\bar{\rho}\left\langle \frac{\partial u'}{\partial t} \right\rangle_y + \bar{\rho}\left\langle \frac{\partial}{\partial x}(\bar{u}u') \right\rangle_y + \bar{\rho}\left\langle \bar{v}\frac{\partial u'}{\partial y} \right\rangle_y + \left\langle \bar{\rho}v'\frac{\partial \bar{u}}{\partial y} \right\rangle_y + \left\langle \frac{\partial p'}{\partial x} \right\rangle_y = 0 \quad (24)$$

Assuming that the flow is isentropic, that the oscillations are one dimensional (i.e., nearly planar), neglecting spatial variations in the mean pressure and density that are second-order in the mean Mach number, and defining α as the isentropic speed of sound, Eq. (23) can be simplified to the following form:

$$\frac{1}{a^2}\frac{\partial p'}{\partial t} + \bar{\rho}\frac{\partial}{\partial x}\langle u'\rangle_y + \frac{p'}{a^2}\frac{\partial}{\partial x}\langle \bar{u}\rangle_y + \frac{1}{a^2}\langle \bar{u}\rangle_y\frac{\partial p'}{\partial x} = -\frac{1}{H}\left[\bar{\rho}v' + \frac{p'\bar{v}}{a^2}\right]_0^H \quad (25)$$

Several important differences exist between the behavior of the investigated experimental setup and that of an unstable solid rocket that affected the nature of the simulation. First, in the present study, the flow turning loss was investigated in an externally driven experiment whose oscillations were excited by acoustic drivers, while an unstable rocket motor is a self-excited system whose amplitude generally increases in the initial, linear, phase of instability. The value of α for the oscillations in the experimental setup is identically zero, because the externally driven oscillations are of constant amplitude. On the other hand, the growth rate α in an actual solid rocket motor is determined by Eq. (14). Another difference is that the frequency of the oscillations in the experimental setup is known (i.e., it is chosen by the experimenter, and need not be a natural frequency of the setup), whereas the frequency of oscillations in an unstable rocket motor is determined by the motor design and operating conditions (e.g., geometry, temperature distribution, boundary conditions and phase difference between the combustion process heat addition and pressure oscillations). With this in mind, the solutions of Eqs. (24) and (25) were assumed to be harmonic, constant amplitude oscillations.

Measured values of the mean axial velocity component at the initial axial boundary of the control volume, the amplitudes and phases of the axial acoustic velocities at the entrance and exit of the investigated control volume, the mean vertical velocity component, and the amplitudes and phases of the vertical acoustic velocities along the top and bottom boundaries of the investigated control volume were used as boundary conditions for the numerical simulation. A shooting method was used to determine the solutions for the acoustic velocity and pressure that minimized the errors at the axial boundaries in a least-squares sense. These values of velocity and pressure

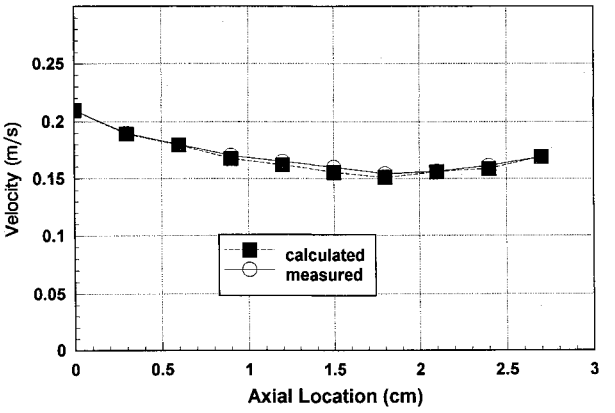

Fig. 8 Comparison of the measured and calculated magnitudes of axial acoustic velocity.

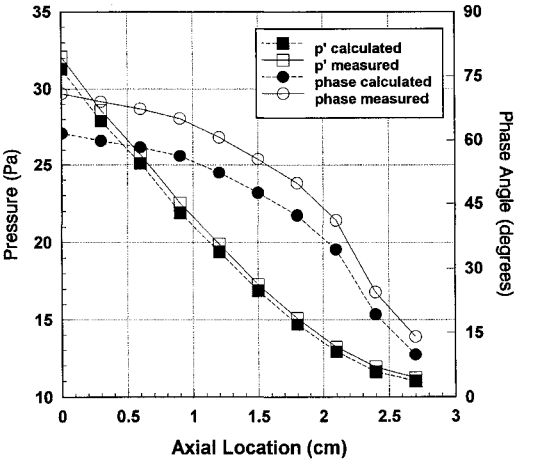

Fig. 9 Comparison of the measured and calculated amplitude and phase of the acoustic pressure.

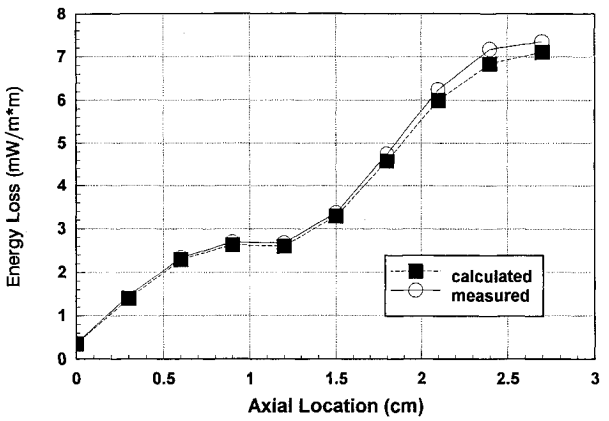

Fig. 10 Comparison of the calculated and measured values of the flow turning loss term.

were then substituted into Eq. (14) to determine the values of the various terms in the acoustic stability equation.

The results of a typical simulation are presented in Figs. 8–10. The measured and calculated values of the axial acoustic velocity are shown in Fig. 8 for an experiment in which the injection velocity V_b was 1.12 m/s, the mean core flow velocity V_c was 2.95 m/s, the frequency was 550 Hz, and injection occurred between a pressure node and antinode. The calculated values match the measured values quite well. Figure 9 shows comparisons between measured and calculated acoustic pressure amplitudes and the phase angles between the pressure and axial velocity oscillations. Figure 9 shows that while the measured and predicted amplitudes are in good agreement, the simulation significantly overpredicts the phase angles. The calculated and measured values of the flow turning loss for this test configuration are presented in Fig. 10, which shows excellent agreement between the predicted and measured values.

Concluding Remarks

Many difficulties exist in the simulation of real motors in the laboratory. In the experimental setup used in this study, the terms proportional to the mean Mach number (such as the flow turning term) were found to be much smaller than the Mach number independent terms (i.e., the classical acoustic intensity terms). This is because the side wall injector had a high acoustic admittance and absorbed a large amount of acoustic energy. In actual solid rocket motors, the response of the propellant is relatively small compared to that of the wall injector. The flow turning losses and other terms proportional to the mean Mach number are often significant and of the same magnitude as the propellant response terms. Another major difference between the experimental injector and an actual solid propellant is that the responses are generally out of phase. While the flow through the injector is generally maximum when the pressure above the burner is low, the burning rate of a solid propellant is, in general, maximum at high pressure. While the theoretical analysis performed in this study is applicable to both the experimental setup and an actual rocket motor, the effects of the differences between the real and modeled flows upon the experimental results are difficult to predict. Unfortunately, laboratory models of solid rockets that correct these problems without creating different ones are unavailable.

With this in mind, experiments have shown the flow turning loss to be linearly dependent upon the side wall injection velocity, which corresponds to the propellant burning rate in an actual solid propellant rocket motor. When the core flow velocity was increased, the magnitude of the flow turning loss increased toward a limiting value that depended upon other experimental conditions. It was determined, however, that the increased flow turning loss was due to incomplete turning of the flow in the investigated region, and under conditions encountered in actual motors, the magnitude of the flow turning loss in a region of the motor is predicted to be independent of the local core flow velocity. The study has shown that the flow turning loss is maximum and minimum when the side wall injection occurs in the vicinity of an acoustic pressure node and antinode, respectively.

Acknowledgments

This research was supported by the Air Force Office of Scientific Research, Bolling AFB, Washington, DC, under Contract 91-0160, and monitored by M. A. Birkan.

References

[1]McClure, F. T., Hart, R. W., and Cantrell, R. H., "Interaction Between Sound and Flow: Stability of T-Burners," *AIAA Journal*, Vol. 1, No. 3, 1963, pp. 586–590.

[2]Derr, R. L., Mathes, H. B., and Crump, J. E., "Application of Combustion Instability Research to Solid Rocket Motor Problems," 53rd Meeting of the NATO AGARD Propulsion and Energetics Panel, Oslo, Norway, 1979.

[3]Baum, J. D., "Acoustic Energy Exchange Through Flow Turning," AIAA Paper 87-0217, 1987.

[4]Sutton, G. P., *Rocket Propulsion Elements*, 5th ed., Wiley, New York, 1986, pp. 310–312.

[5]Culick, F. E. C., "The Stability of One Dimensional Motions in a Rocket Motor," *Combustion Science and Technology*, Vol. 7, No. 4, 1973, pp. 165–175.

[6]Culick, F. E. C., "Stability of Three-Dimensional Motions in a Combustion Chamber," *Combustion Science and Technology*, Vol. 10, No. 3, 1975, pp. 109–124.

[7]Culick, F. E. C., "Remarks on Entropy Production in the One-Dimensional Approximations to Unsteady Flow in Combustion Chambers," *Combustion Science and Technology*, Vol. 15, No. 3, 1977, pp. 93–97.

[8]Culick, F. E. C., Magiawala, K., Wat, J., Awad, E., and Kubota, T., "Measurements of Energy Losses Associated with Interactions Between Acoustic Waves and Non-Uniform Steady Flow," Air Force Rocket Propulsion Rept. TR-81-22, July 1981.

[9]Hersch, A. S., and Walker, B., "Experimental Investigation of Rocket Motor Flow Turning Losses," AIAA Paper 83-1267, June 1983.

[10]Hersch, A. S., and Tso, J., "Flow Turning Losses in Solid Rocket Motors," Air Force Astronautics Lab. Rept. TR-095, March 1988.

[11]Chen, T., "Driving of Axial Acoustic Fields by Sidewall Stabilized Diffusion Flames," Ph.D. Dissertation, Georgia Inst. of Technology, Atlanta, GA, July 1990.

[12]Baum, J. D., and Levine, J. N., "Acoustic-Mean Flow Interaction," AFRPL-TR-86-065, Jan. 1987.

[13]Baum, J. D., "Numerical Investigation of Energy Exchange Mechanisms Between Mean and Acoustic Flow Fields in a Simulated Rocket Combustor," AIAA Paper 90-2310, 1990.

[14]Hegde, U. G., Chen, F., and Zinn, B. T., "Investigation of the Acoustic Boundary Layer in Porous Walled Ducts with Flow," *AIAA Journal*, Vol. 24, No. 9, 1986, pp. 1474–1482.

[15]Hegde, U. G., and Zinn, B. T., "Rocket Motor Flow Turning Losses," *AIAA Journal*, Vol. 24, No. 8, 1986, pp. 1394–1396.

[16]Hegde, U. G., and Zinn, B. T., "The Acoustic Boundary Layer in Porous Walled Ducts with a Reacting Flow," *Proceedings of the 21st Symposium on Combustion*, The Combustion Inst., Pittsburgh, PA, 1986, pp. 1993–2000.

[17]Cantrell, R. H., and Hart, R. W., "Interactions Between Sound and Flow in Acoustic Cavities: Mass, Momentum, and Energy Considerations," *Journal of the Acoustical Society of America*, Vol. 36, No. 4, 1964, pp. 697–706.

[18]Flandro, G. A., "Stability Prediction for Solid Propellant Rocket Motors with High Speed Mean Flow," AFRPL TR-79-98, 1980.

[19]Matta, L. M., "Investigation of the Flow Turning Loss in Unstable Solid Propellant Rocket Motors," Ph.D. Dissertation, Georgia Inst. of Technology, Atlanta, GA, Dec. 1993.